Rev.Adv.Mater.Sci. 15(2007) 49-55

X-RAY MICROBEAM CHARACTERIZATION OF THE NEAR SURFACE NANOSTRUCTURED LAYER IN Ti AFTER FRICTION STIR PROCESSING

O.M. Barabash, R.I. Barabash, G.E. Ice, S.A. David, Z. Feng and J. Horton

Materials Science and Technology Div., Oak Ridge National Laboratory, One Bethel Valley Road, Oak Ridge TN 37831, USA

Received: January 22, 2007

Abstract. Plastic deformation and structural changes of a Ti surface after Friction Stir Processing (FSP) were analyzed by means of SEM, EBSD and advanced 3D polychromatic X-ray micro diffraction at the APS synchrotron. Spatially resolved 3D Laue diffraction allowed observing the changes in dislocation arrangement with depth in different regions of the FSP Ti. Formation of two specific zones was established: friction stir zone (FSZ), with an average thickness of 300 μm, and thermomechanicaly affected zone (TMAZ) with a thickness of 800 μm. It was shown that FSP generates a large number of dislocations. Maximal dislocation density is located within the TMAZ. Dislocation density gradually decreases and reaches the value typical for base metal. Within the TMAZ dislocations are distributed inhomogeneously. Inhomogeneity of plastic deformation and dislocations arrangement is found in 3D both within the individual grains and between separate grains.

1. INTRODUCTION

Currently, nanostructured materials are a subject of intensive research [1–11]. Special attention is devoted to formation of a nanostructural state in bulk materials. It has been established, that two main phenomena determine formation of the micron and submicron size grains: (1) initial inhomogeneous (with a direction change) plastic deformation; and (2) recrystallization (nucleation and growth) of small size grains [8]. Friction stir processing (FSP) is recently an intensively developing method of thermo-mechanical treatment of different materials. It includes high speed inhomogeneous plastic deformation. During FSP a special tool (Fig. 1) is moving along certain direction being loaded in close contact with the surface of the treated material and simultaneously rotating with high speed around its axis [1,5,6]. Depending on the purpose and material for FSP, the size and shape of the tool varies. Rotation together with longitudinal movement result in the high speed plastic deformation that is spatially inhomogeneous. Essential mass transfer is observed in the rotation region of the tool [5,6]. A special structure, termed stir zone, (SZ) is formed as a result of this process. Usually recrystallization takes place simultaneously with plastic deformation in the SZ. Recrystallization accompanies plastic deformation; however it can stop at different stages depending on the FSP parameters and nature of the treated material. FSP allows: (1) creation of ultra fine grained bulk materials in a single step; (2) easy parameter control over broad intervals; (3)

Corresponding author: O.M. Barabash, e-mail: barabashom@ornl.gov

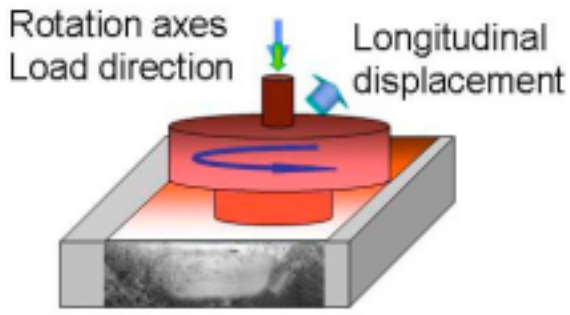

Fig. 1. Schematic of the tool arrangement for friction stir processing providing rotation around the axes in contact with the surface of the processed material and longitudinal movement along the surface of the material.

multipasses to form extended nanostructured regions near the surface [5,6]; (4) for treatment of high strength steels and alloys [8]; (5) is relatively inexpensive. Local inhomogeneity is the most distinct feature of the microstructure in the SZ. This study is focused on the possibility of the formation of a nanostructural state in the near surface stir zone as well as on the analysis of inhomogeneities in different zones in the α-titanium after FSP.

2. EXPERIMENTAL DETAILS

Analysis of the strain, dislocation distribution and lattice rotations was performed with white microbeam Laue diffraction. X-ray microbeam measurement of dislocation structures is an emerging new area of microbeam diffraction. The techniques are based on classic polychromatic (white) beam Laue diffraction (PXM), which is widely used to determine crystal symmetry and orientation and deviatoric macrostrains. Compared to traditional monochromatic microbeam diffraction the white-beam method has several advantages [12-15]: (1) the sample does not need to be rotated which is important because the sphere of confusion of a typical goniometer limits measurements at a submicron scale; (2) the intensity distributions around a large number of different reflections can be simultaneously analyzed from the same subgrain; and (3) an uncompromised full three-dimensional reciprocal space intensity distribution can be measured when necessary by scanning the incident beam energy.

For microbeam diffraction it is most convenient to operate with the detector near 2θ~90° (Fig. 2). Because X-rays are penetrating, an X-ray microbeam experiment produces a Laue pattern from every fragment or cell that it intercepts along its path. These overlapping Laue patterns can be separated by triangulation or other techniques [12-

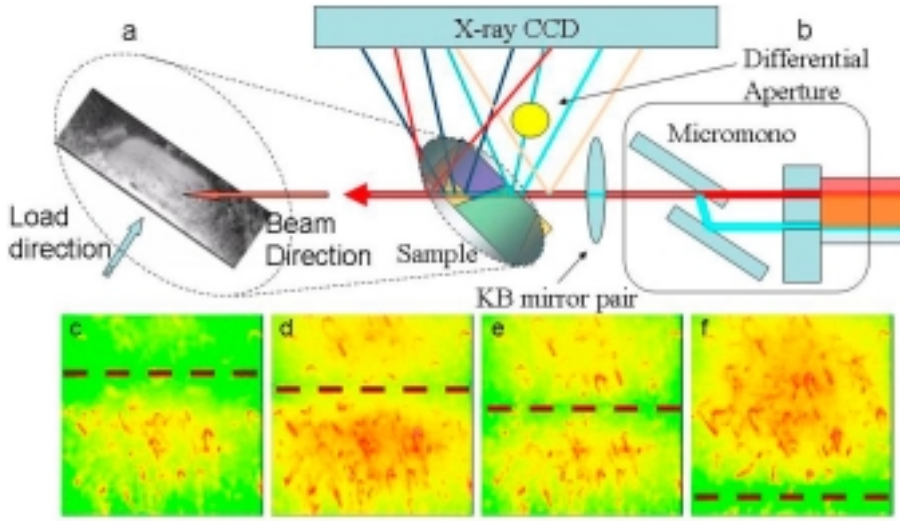

Fig. 2. Schematic of the sample orientation relative to the microbeam (a); geometry of PXM and DAXM (b); several “raw” Laue patterns shadowed with different wire positions, which are further used to create the reconstructed images corresponding to the intensity from certain depth (c –f). Positions of the wire shadow in (c – f) are indicated by dashed lines.

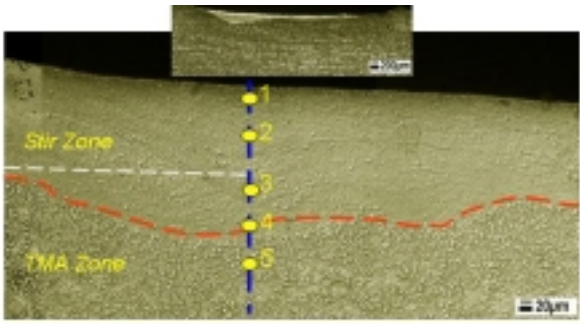

Fig. 3. General view (OM) of the microstructure in the stir and the thermomechanically affected zones in the Ti after FSP.

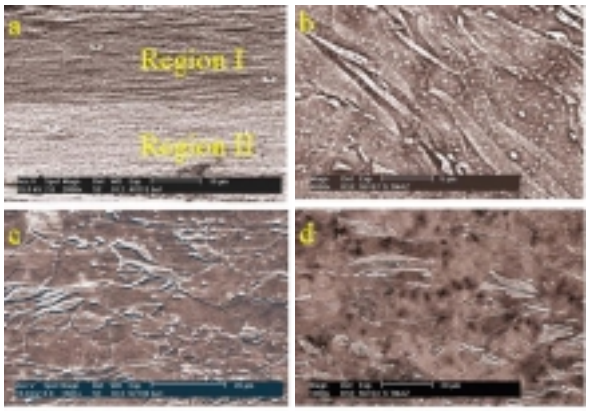

Fig. 4. Microstructure (SEM) at a depth of 50 μm at the border region between two different regions in the stir zone (a); in the immediate vicinity of the border region between stir zone and TMAZ (b), 600 μm from the SZ into the TMAZ (c); 900 μm from the SZ into the TMAZ (d).

14]. To get depth resolved information about the strain distribution in the Ti layers we performed measurements with the so-called DAXM technique [13] (Fig. 2b – f). A smooth absorbing wire translates parallel to the sample surface. If the wire is moved a small increment near the sample surface, the change in the Laue pattern arises from X-rays that pass near the leading or trailing edge of the wire. At different positions wire is shadowing different portions of the Laue diffraction image (Figs. 2c – 2f). By following the intensity changes in each CCD pixel, one can construct the subgrain Laue patterns [13].

Differential aperture microscopy (DAXM) can often resolve a Laue image into single crystal-like patterns. However, when the density of dislocations is high, streaking is observed even in thin films and for DAXM resolved patterns. Typically streaking in Laue patterns indicates the presence of lattice rotations as a result of unpaired or “geometrically necessary” dislocations [14,15]. However, streaking can also result from gradients in the elastic strain tensor as illustrated in an experiment on bent Si single crystal by Larson *et al.*, [13]. For PXM analysis, the samples with the thickness of ~1000 μm (which is less then the penetration depth in Ti for the upper value energy of the beam) were cut from the Ti after FSP perpendicular to the displacement direction of the tool. Microdiffraction patterns with a beam diameter of either 0.5 μm or 0.08 μm and with an incident angle of 45° and CCD detector at 90° were taken at 400 different locations with a step size of 10 μm along four different lines with the distance of 100 μm between the lines within the stir and thermomechanically affected zones.

The samples for optical microscopy analysis were conventionally polished and etched in a solution of 5 ml HNO_3, 100 ml H_2O, and 5 ml HF. Samples for orientation imaging microscopy (OIM) and TEM investigations were electropolished in a solution of 10 ml perchloric acid (70%) and 90 ml methanol at -30 °C, 13 V, and 30V. TEM observations are carried out with a TECHNAI 20 transmission electron microscope operated at 200 kV. The OIM is carried out with a Scanning Electron Microscopy (SEM). Observations have been performed in a Philips XL 30 SEM-FEG microscope integrated with a computer aided EBSD system from TSL OIM 4.5 operating at 20 kV.

For this study FSP of polycrystalline titanium was performed with one friction stir pass.

3. RESULTS AND DISCUSSION

A general view of the Ti sample after FSP is shown in Fig. 3. Several distinct zones are observed: a stir zone (SZ) with the total length of 350 μm, a thermo-mechanically affected zone (TMAZ) and heat affected zone (HAZ) (Fig. 3). Two regions are further distinguished within the stir zone (Fig. 4a). The first region with the width of 50 mm is followed by the second region down to a depth of 350 μm.

Both in-plane rotational and vortex modes of plastic deformation are observed in the SZ and TMAZ (Figs. 4c – 4d). All zones are characterized with distinct structure. They may be described with a number of distinct parameters. Before FSP the

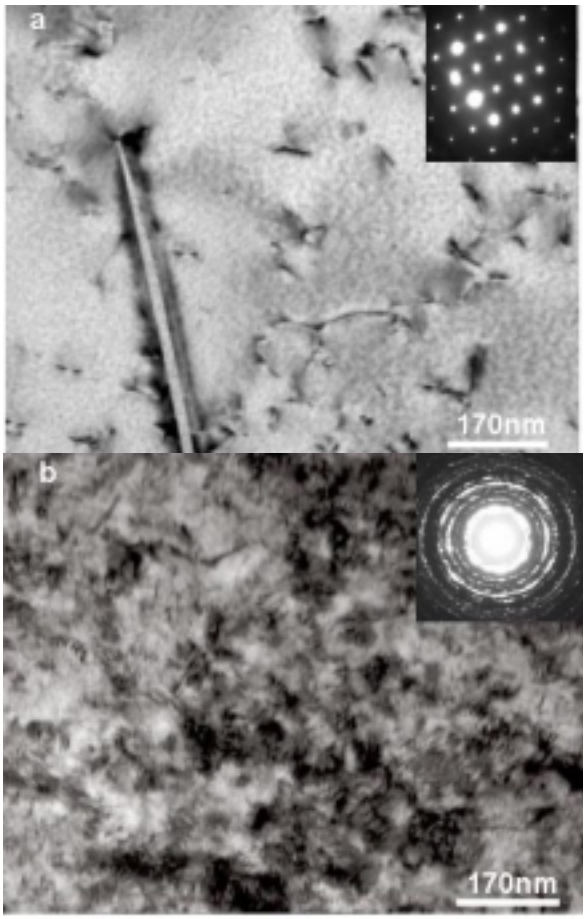

Fig. 5. TEM images of the base materials before friction stir processing with a diffraction pattern from one grain (a) and dislocation forest in the stir zone with diffraction rings from the nanocrystalline grains (b).

structure of polycrystalline α-Ti consists of large grains (average size of ~ 12 μm) with very low dislocation density. After FSP in the stir zone, TEM analysis reveals a high dislocation density and a small grain size (Fig. 5) below the resolution limit of the OIM and SEM analysis. The structure of the stir and thermomechanically affected zones was further characterized by polychromatic (PXM) and monochromatic micro diffraction synchrotron analysis (Fig. 6). The Laue patterns from the stir zone (Figs. 6a and 6b) were obtained with nano size (~ 80 nm) polychromatic beam. Similar images were obtained from the TMAZ with submicron (~ 0.5 μm) beam. All images demonstrate intensive streaking, which is a signature of strong lattice curvature caused by geometrically necessary (GN) dislocations and deviatoric strain within the probed region [12,13]. Due to high energy of the beam (7 - 25) keV, they penetrate through the sample and give an information from different depths of the sample. Specimen penetration depth is 80 - 100 μm. The sample was oriented relative to the beam in a way that the beam penetrates the layers located at the same distance from the surface. This way each Laue pattern gives information about the structure typical for a certain depth under the surface (Fig. 6).

Near the very surface (region I of the stir zone) even the nanosize Laue beam did not resolve the structure, and further characterization of this region was performed with monochromatic beam at an energy of ~15.4 keV with submicron (~ 0.5 μm) beam (Figs. 7 and 8). In the diffraction pattern obtained from the surface (region I) - (Fig. 7a) the set of diffraction peaks corresponding to the α - Ti is overlapping with a broad diffraction “halo” typical for diffraction from amorphous materials. At a depth of 25 μm (Fig. 7b) the intensity of the “amorphous halo” slightly decreases. The intensity remains approximately the same even at a depth of 100 μm within the stir zone (Fig. 8a). When the probing location approaches TMAZ the “amorphous halo”

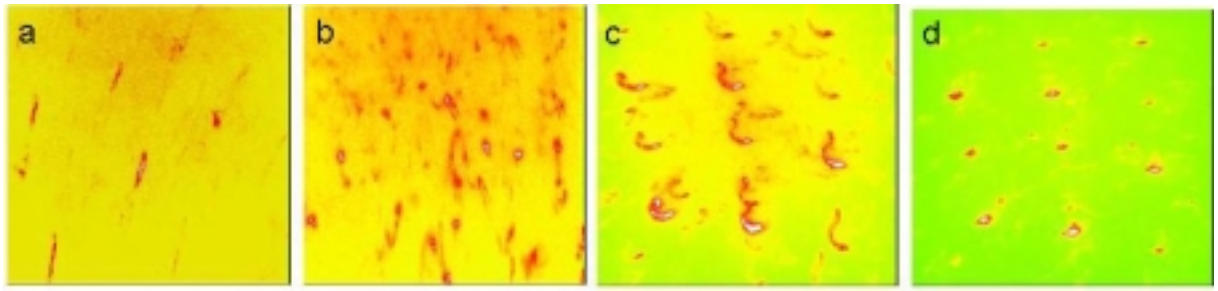

Fig. 6. Typical Laue patterns obtained with the nanosize polychromatic beam from different locations in the stir zone (a, b) and in the TMAZ obtained with a submicron (~0.5 μm) polychromatic beam (c, d) show intensive (~2 -3°) lattice rotations within individual submicron size grains.

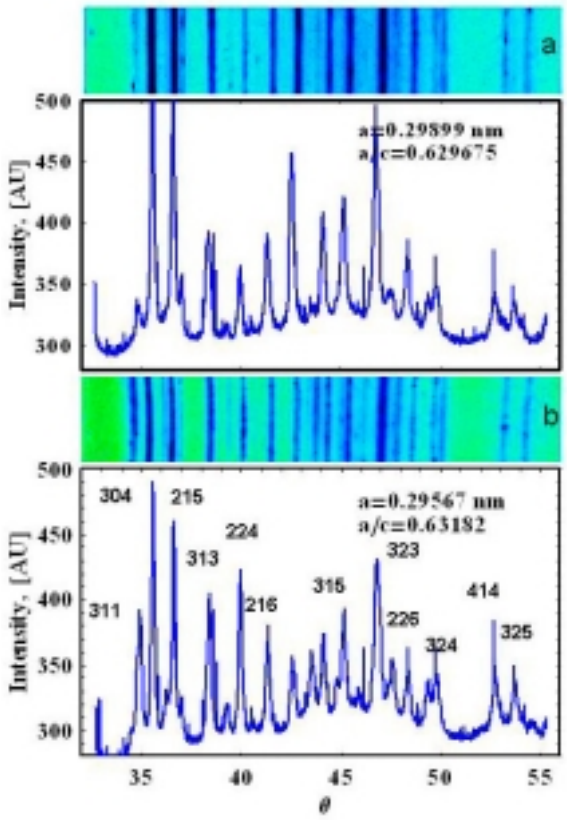

Fig. 7. Monochromatic micro diffraction patterns (beam size ~0.5μm, energy 15.4 keV) from the 1st region of the stir zone at the surface region (a) and at a depth of 25 μm (b) show formation of nanosized α-Ti grain together with deformation-disordered amorphous component in the near surface region. Miller indices for different *hkl* are indicated in (b).

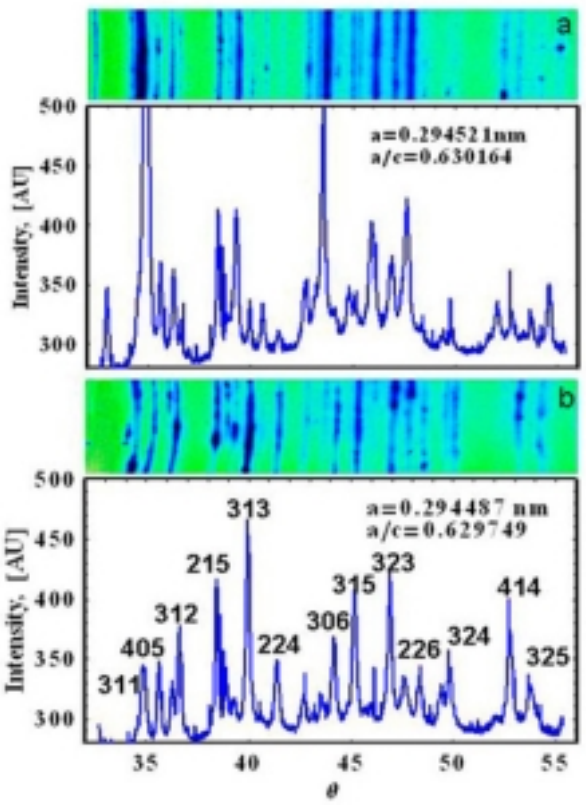

Fig. 8. Monochromatic micro diffraction patterns (beam size ~0.5 μm, energy 15.4 keV) from the 2nd region of the stir zone at the depth of 100 μm (a) and from the TMAZ at a depth of 450 μm (b) show a decrease of the amorphous component with depth and increase of α-Ti grain size. Miller indices for different *hkl* are indicated in (b).

practically disappeared (Fig. 8b). The diffraction pattern become very spiky. Individual diffraction spots were resolved within each *hkl* diffraction ring. The size of coherently scattering cell blocks was determined with line profile analysis [14 - 25] of the diffraction maxima (Figs. 7 and 8). Within the 1st region of the stir zone, it is equal to ~ 14 nm. In the 2nd region of the stir zone, it increases up to ~ 20 nm. According to TEM analysis, the grain sizes in the stir zone is about 30 – 60 nm (Fig. 5b). This indicated that due to the severe deformation the nanosize grains in the stir zone have a sub-structure, and consisted of several coherently scattering regions.

In the TMAZ (located within the depth interval of 350-1000 μm) the Laue patterns are heavily streaked indicating strong rotational and vortex deformation modes even within individual grains (Fig. 6c, 6d, and Fig. 9). These patterns are very complicated as the diffraction patterns obtained from different grains are overlapped. These patterns were disentangled with the DAXM technique [11-13]. The spatially resolved images corresponding to a one micron step size demonstrated intensive lattice rotations within each grain (Fig. 9). Several different grains are intercepted by the beam. The change from one grain to another took place on average within 6 microns. However, strong lattice rotations (several degrees) are observed even within each grain.

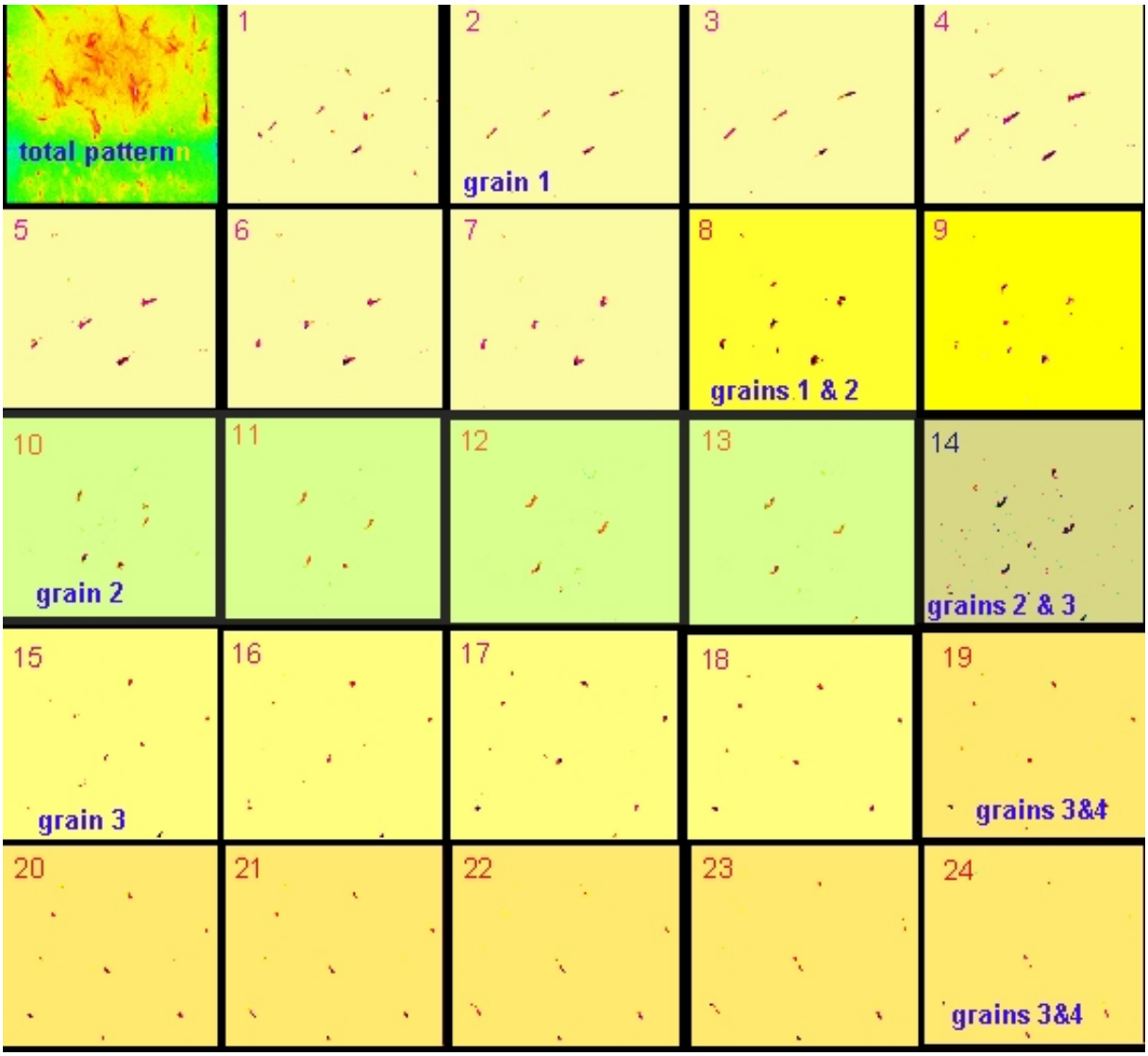

Fig. 9. A series of depth resolved Laue patterns with the depth in μm indicated in each pattern. The top left corner shows a total depth integrated Laue pattern. These results show lattice rotations within individual submicron grains as a function of depth.

4. CONCLUSIONS

· After FSP, the stir zone in polycrystalline Ti consisted of two distinct regions with a different size of nanocrystalline grains mixed with an amorphous component.

· Rotational and vortex deformation modes are observed within thermomechanically affected zone.

· Lattice rotations were observed both within individual grains and between grains.

· The deformation in the neighbor grains was distinct and depended on their orientation and internal stresses between surrounding grains.

ACKNOWLEDGEMENT

Research sponsored by the Division of Materials Sciences and Engineering, Office of Basic Energy Sciences and the ORNL SHARE user facility, U.S. Department of Energy, under Contract DE-AC05-00OR22725 with UT-Battelle, LLC. Work in part on Unicat beamline 34-ID at the Advanced Photon

Source (APS), which is supported by the University of Illinois at Urbana-Champaign, Materials Research Laboratory (U.S. DOE, the State of Illinois-IBHE-HECA, and the NSF), and by the Oak Ridge National Laboratory (U.S. DOE under contract with UT-Battelle LLC). The APS is supported by the U.S. DOE, Basic Energy Sciences, Office of Science under contract No. W-31-109-ENG-38.

REFERENCES

[1] P.B. Berbon, W. H. Bingel, R.S. Mishra, C.C. Bampton and M.W. Mahoney // *Scripta Mater.* **44** (2001) 61.
[2] J.-Q. Su, T. W. Nelson and C.J. Sterling // *J.Mater.Res.* **18** (2003) 1757.
[3] F. Sun, P. Rojas, A. Zuniga and E.J. Lavernia // *Mater.Sci.Eng. A*, in print.
[4] C. Genevois, A. Deschamps and P. Vacher // *Mater.Sci.Eng. A* **415** (2006) 162.
[5] Z.Y. Ma, S.R. Sharma and R.S. Mishra // *Mater.Sci.Eng. A*, in print.
[6] R.S. Mishra and Z.Y. Ma // *Mater.Sci.Eng. R* **50** (2005) 1.
[7] K.Y. Zhu, A. Vassel, F. Brisset, K. Lu and J. Lu // *Acta Mater.* **52** (2004) 4101.
[8] R. Valiev // *Nature Mater* **3** (2004) 511; *Adv.Eng.Mater.* **5** (2003) 296.
[9] Y.T. Zhu and X. Liao // *Nature Mater* **3** (2004) 351.
[10] Y.T. Zhu, J.Y. Huang, J. Gubicza, T. Ungar, Y.M. Wang, E. Ma and R.Z. Valiev // *J.Mater.Res.* **18** (2003) 1908.
[11] H.V.Swygenhoven // *Science* **296** (2002) 66.
[12] N. Tamura, H.A. Padmore and J.R. Patel // *Mater.Sci. Engineer. A* **399** (2005) 92.
[13] B.C. Larson, W. Yang, G.E. Ice, J.D. Budai and J.Z. Tischler // *Nature* **415** (2002) 887.
[14] R.I. Barabash and G.E. Ice, In: *Encyclopedia of Materials: Science and Technology Updates* (Elsevier, Oxford, 2005) p. 1.
[15] G. Ice, R. Barabash and F. Walker // *J. Appl. Physics* **93** (2003) 1457.
[16] T. Ungar, G. Tichi, J. Gubicza and R.J. Hellmig // *Powder Diffraction* **20** (2005) 366.
[17] H.G. Jiang, M. Ruhle and E.J. Lavernia // *J.Mater.Res.* **14** (1999) 549.
[18] R.I. Barabash and P. Klimanek // *Zeitschrift fur Metallkunde* **1** (2001) 70.
[19] R.I. Barabash and P. Klimanek // *J. Appl. Cryst.* **32** (1999) 1050.
[20] M.A. Krivoglaz, K.P. Ryaboshapka and R.I. Barabash // *Fiz.Metal.Metallov.* **30** (1970) 1134.
[21] M.A. Krivoglaz, *X-ray and Neutron Diffraction in Nonideal Crystals* (Springer, Berlin, 1996); *Theory of X-ray and Thermal Neutron Scattering by Real Crystals* (Plenum, New York, 1969).
[22] M. Wilkens, *Fundamental Aspects of Dislocation Theory* (National Bureau of Standards Special Publication, Washington, DC) **II**, 317 (1970) 1195pp.
[23] H. Mughrabi and T. Ungar // *Nature Mater* **5** (2006) 601.
[24] H. Mughrabi // *Acta Mater* **54** (2006) 3417.
[25] H. Mughrabi // *Acta Metall.* **31** (1980) 1367.
[26] M. Wilkens, T. Ungar and H. Mughrabi // *Phys. Stat. Sol. (a)* **104** (1987) 157.
[27] M. Leoni and P. Scardi // *J.Appl.Cryst.* **37** (2004) 629.